

NETWORK SCIENCE

Higher-order organization of complex networks

Austin R. Benson,¹ David F. Gleich,² Jure Leskovec^{3*}

Networks are a fundamental tool for understanding and modeling complex systems in physics, biology, neuroscience, engineering, and social science. Many networks are known to exhibit rich, lower-order connectivity patterns that can be captured at the level of individual nodes and edges. However, higher-order organization of complex networks—at the level of small network subgraphs—remains largely unknown. Here, we develop a generalized framework for clustering networks on the basis of higher-order connectivity patterns. This framework provides mathematical guarantees on the optimality of obtained clusters and scales to networks with billions of edges. The framework reveals higher-order organization in a number of networks, including information propagation units in neuronal networks and hub structure in transportation networks. Results show that networks exhibit rich higher-order organizational structures that are exposed by clustering based on higher-order connectivity patterns.

Networks are a standard representation of data throughout the sciences, and higher-order connectivity patterns are essential to understanding the fundamental structures that control and mediate the behavior of many complex systems (1–7). The most common higher-order structures are small network subgraphs, which we refer to as network motifs (Fig. 1A). Network motifs are considered building blocks for complex networks (1, 8). For example, feed-forward loops (Fig. 1A, M_5) have proven fundamental to understanding transcriptional regulation networks (9); triangular motifs (Fig. 1A, M_1 – M_7) are crucial for social networks (4); open bidirectional wedges (Fig. 1A, M_{13}) are key to structural hubs in the brain (10); and two-hop paths (Fig. 1A, M_8 – M_{13}) are essential to understanding air traffic patterns (5). Although network motifs have been recognized as fundamental units of networks, the higher-order organization of networks at the level of network motifs largely remains an open question.

Here, we use higher-order network structures to gain new insights into the organization of complex systems. We develop a framework that identifies clusters of network motifs. For each network motif (Fig. 1A), a different higher-order clustering may be revealed (Fig. 1B), which means that different organizational patterns are exposed, depending on the chosen motif.

Conceptually, given a network motif M , our framework searches for a cluster of nodes S with two goals. First, the nodes in S should participate in many instances of M . Second, the set S should avoid cutting instances of M , which occurs when only a subset of the nodes from a motif are in the set S (Fig. 1B). More precisely, given a motif M , the higher-order clustering framework aims to find a cluster (defined by a set of nodes S) that

minimizes the following ratio:

$$\phi_M(S) = \text{cut}_M(S, \bar{S}) / \min[\text{vol}_M(S), \text{vol}_M(\bar{S})] \quad (1)$$

where \bar{S} denotes the remainder of the nodes (the complement of S), $\text{cut}_M(S, \bar{S})$ is the number of instances of motif M with at least one node in S and one in \bar{S} , and $\text{vol}_M(S)$ is the number of nodes

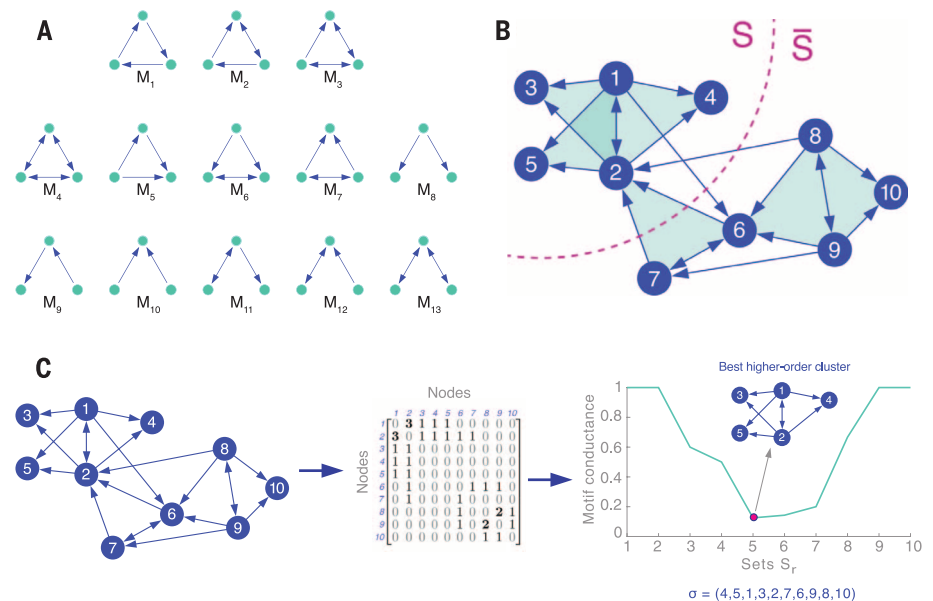


Fig. 1. Higher-order network structures and the higher-order network clustering framework.

(A) Higher-order structures are captured by network motifs. For example, all 13 connected three-node directed motifs are shown here. (B) Clustering of a network based on motif M_7 . For a given motif M , our framework aims to find a set of nodes S that minimizes motif conductance, $\phi_M(S)$, which we define as the ratio of the number of motifs cut (filled triangles cut) to the minimum number of nodes in instances of the motif in either S or \bar{S} (13). In this case, there is one motif cut. (C) The higher-order network clustering framework. Given a graph and a motif of interest (in this case, M_7), the framework forms a motif adjacency matrix (W_M) by counting the number of times two nodes co-occur in an instance of the motif. An eigenvector of a Laplacian transformation of the motif adjacency matrix is then computed. The ordering σ of the nodes provided by the components of the eigenvector (15) produces nested sets $S_r = \{\sigma_1, \dots, \sigma_r\}$ of increasing size r . We prove that the set S_r with the smallest motif-based conductance, $\phi_M(S_r)$, is a near-optimal higher-order cluster (13).

¹Institute for Computational and Mathematical Engineering, Stanford University, Stanford, CA 94305, USA. ²Department of Computer Science, Purdue University, West Lafayette, IN 47906, USA. ³Computer Science Department, Stanford University, Stanford, CA 94305, USA.

*Corresponding author. Email: jure@cs.stanford.edu

in instances of M that reside in S . Equation 1 is a generalization of the conductance metric in spectral graph theory, one of the most useful graph partitioning scores (11). We refer to $\phi_M(S)$ as the motif conductance of S with respect to M .

Finding the exact set of nodes S that minimizes the motif conductance is computationally infeasible (12). To approximately minimize Eq. 1 and, hence, to identify higher-order clusters, we developed an optimization framework that provably finds near-optimal clusters [supplementary materials (13)]. We extend the spectral graph clustering methodology, which is based on the eigenvalues and eigenvectors of matrices associated with the graph (12), to account for higher-order structures in networks. The resulting method maintains the properties of traditional spectral graph clustering: computational efficiency, ease of implementation, and mathematical guarantees on the near-optimality of obtained clusters. Specifically, the clusters identified by our higher-order clustering framework satisfy the motif Cheeger inequality (14), which means that our optimization framework finds clusters that are at most a quadratic factor away from optimal.

The algorithm (illustrated in Fig. 1C) efficiently identifies a cluster of nodes S as follows:

- **Step 1:** Given a network and a motif M of interest, form the motif adjacency matrix W_M whose entries (i, j) are the co-occurrence counts of nodes i and j in the motif M : $(W_M)_{ij}$ = number of instances of M that contain nodes i and j .

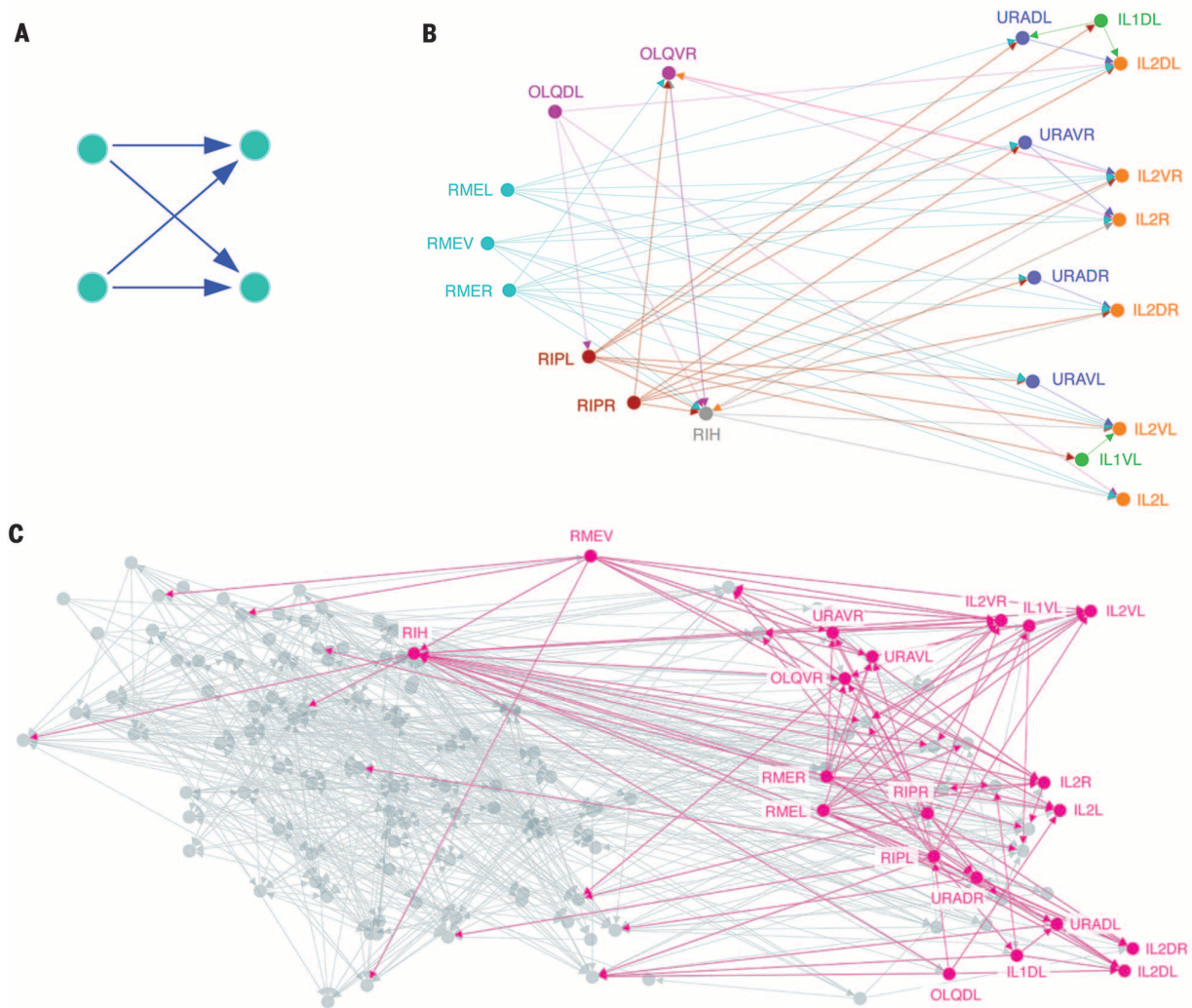


Fig. 2. Higher-order cluster in the *C. elegans* neuronal network. [See (29).] (A) The four-node bi-fan motif, which is overexpressed in neuronal networks (1). Intuitively, this motif describes a cooperative propagation of information from the nodes on the left to the nodes on the right. (B) The best higher-order cluster in the *C. elegans* frontal neuronal network based on the motif in (A). The cluster contains three ring motor neurons (RME_L, -V, and -R; cyan) with many outgoing connections, which serve as the source of information; six inner labial sensory neurons (IL2_{DL}, -VR, -R, -DR, -VL, and -L; orange) with many incoming connections, serving as the destination of information; and four URA motor neurons (purple) acting as intermediaries. These RME neurons

have been proposed as pioneers for the nerve ring (21), whereas the IL2 neurons are known regulators of nictation (22), and the higher-order cluster exposes their organization. The cluster also reveals that RIH serves as a critical intermediary of information processing. This neuron has incoming links from three RME neurons, outgoing connections to five of the six IL2 neurons, and the largest total number of connections of any neuron in the cluster. (C) Illustration of the higher-order cluster in the context of the entire network. Node locations are the true two-dimensional spatial embedding of the neurons. Most information flows from left to right, and we see that RMEV, -R, and -L and RIH serve as sources of information to the neurons on the right.

• Step 2: Compute the spectral ordering σ of the nodes from the normalized motif Laplacian matrix constructed via W_M (15).

• Step 3: Find the prefix set of σ with the smallest motif conductance (the argument of the minimum), formally, $S := \arg \min_r \phi_M(S_r)$, where $S_r = \{\sigma_1, \dots, \sigma_r\}$.

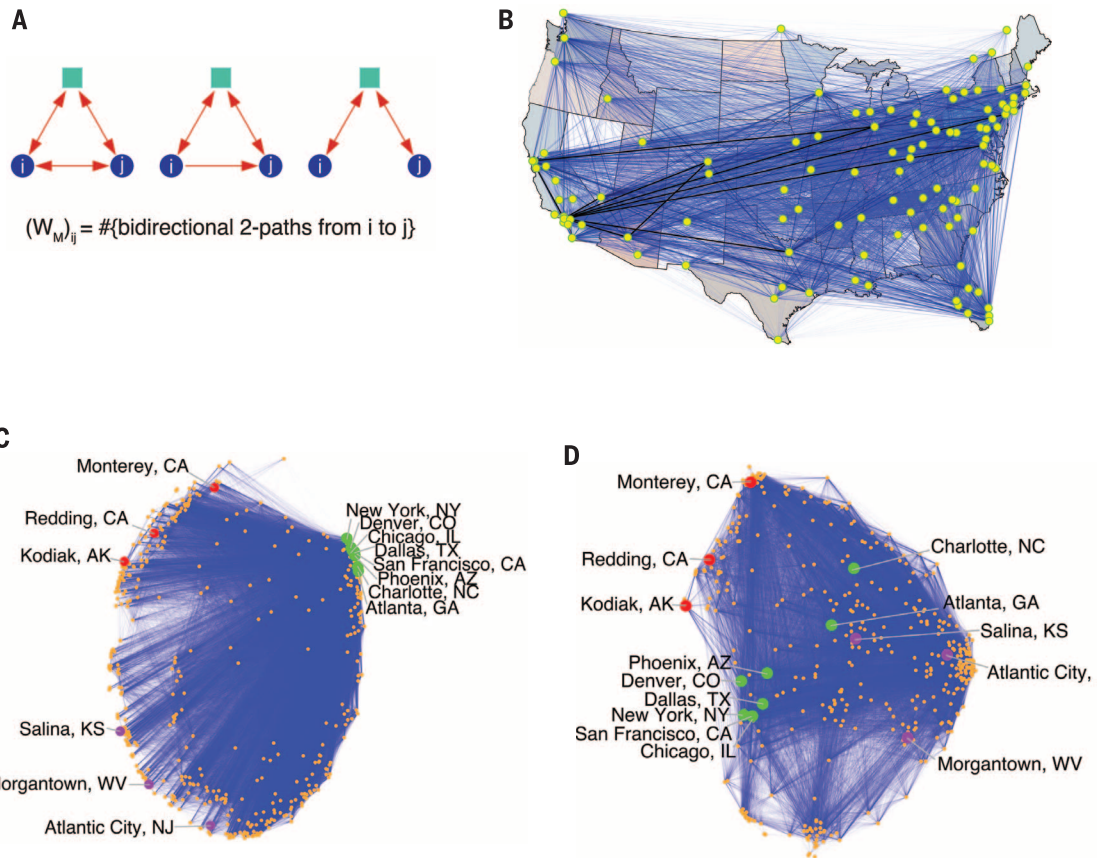
For triangular motifs, the algorithm scales to networks with billions of edges and, typically, only takes several hours to process graphs of such size. On smaller networks with hundreds of thousands of edges, the algorithm can process motifs up to size 9 (13). Although the worst-case computational complexity of the algorithm for triangular motifs is $\Theta(m^{1.5})$, where m is the number of edges

in the network, in practice, the algorithm is much faster. By analyzing 16 real-world networks where the number of edges m ranges from 159,000 to 2 billion, we found the computational complexity to scale as $\Theta(m^{1.2})$. Moreover, the algorithm can easily be parallelized, and sampling techniques can be used to further improve performance (16).

The framework can be applied to directed, undirected, and weighted networks, as well as motifs (13). Moreover, it can also be applied to networks with positive and negative signs on the edges, which are common in social networks (friend versus foe or trust versus distrust edges) and metabolic networks (edges signifying activation versus inhibi-

tion) (13). The framework can be used to identify higher-order structure in networks where domain knowledge suggests the motif of interest. In the supplementary materials, we also show that when a domain-specific higher-order pattern is not known in advance, the framework can also serve to identify which motifs are important for the modular organization of a given network (13). Such a general framework allows complex higher-order organizational structures in a number of different networks by using individual motifs and sets of motifs. The framework and mathematical theory immediately extend to other spectral methods, such as localized algorithms that find clusters around a seed node (17) and

Fig. 3. Higher-order spectral analysis of a network of airports in Canada and the United States. [See (23).] (A) The three higher-order structures used in our analysis. Each motif is “anchored” by the blue nodes i and j , which means our framework only seeks to cluster together the blue nodes. Specifically, the motif adjacency matrix adds weight to the (i, j) edge on the basis of the number of third intermediary nodes (green squares).



$$(W_M)_{ij} = \#\{\text{bidirectional 2-paths from } i \text{ to } j\}$$

(C) Embedding of nodes provided by their corresponding components

of the first two nontrivial eigenvectors of the normalized Laplacian for W_M . The marked cities are eight large U.S. hubs (green), three West Coast nonhubs (red), and three East Coast nonhubs (purple). The primary spectral coordinate (left to right) reveals how much of a hub the city is, and the second spectral coordinate (top to bottom) captures west-east geography (13). (D) Embedding of nodes provided by their corresponding components in the first two nontrivial eigenvectors of the standard, edge-based (non-higher-order) normalized Laplacian. This method does not capture the hub and geography found by the higher-order method. For example, Atlanta, the largest hub, is in the center of the embedding, next to Salina, a nonhub.

algorithms for finding overlapping clusters (18). To find several clusters, one can use embeddings from multiple eigenvectors and k -means clustering (13, 19) or can apply recursive bipartitioning (13, 20).

The framework can serve to identify a higher-order modular organization of networks. We apply the higher-order clustering framework to the *Caenorhabditis elegans* neuronal network, where the four-node “bi-fan” motif (Fig. 2A) is overexpressed (1). The higher-order clustering framework then reveals the organization of the motif within the *C. elegans* neuronal network. We find a cluster of 20 neurons in the frontal section with low bi-fan motif conductance (Fig. 2B). The cluster shows a way that nictation is controlled. Within the cluster, ring motor neurons (RMEL, -V, or -R), proposed pioneers of the nerve ring (21), propagate information to inner labial sensory neurons, regulators of nictation (22), through the neuron RIH (Fig. 2C). Our framework contextualizes the importance of the bi-fan motif in this control mechanism.

The framework also provides new insights into network organization beyond the clustering of nodes based only on edges. Results on a trans-

portation reachability network (23) demonstrate how it finds the essential hub interconnection airports (Fig. 3). These appear as extrema on the primary spectral direction (Fig. 3C) when two-hop motifs (Fig. 3A) are used to capture highly connected nodes and nonhubs. [The first spectral coordinate of the normalized motif Laplacian embedding was positively correlated with the airport city’s metropolitan population with Pearson correlation 99% confidence interval (0.33, 0.53).] The secondary spectral direction identified the west-east geography in the North American flight network [it was negatively correlated with the airport city’s longitude with Pearson correlation 99% confidence interval (−0.66, −0.50)]. On the other hand, edge-based methods conflate geography and hub structure. For example, Atlanta, a large hub, is embedded next to Salina, a nonhub, with an edge-based method (Fig. 3D).

Our higher-order network clustering framework unifies motif analysis and network partitioning—two fundamental tools in network science—and reveals new organizational patterns and modules in complex systems. Prior efforts along these lines do not provide worst-case performance guarantees on the obtained clustering (24) and do not reveal

which motifs organize the network (25) but rely on expanding the size of the network (26, 27). Theoretical results in the supplementary materials (13) also explain why classes of hypergraph partitioning methods are more general than previously assumed and how motif-based clustering provides a rigorous framework for the special case of partitioning directed graphs. Finally, the higher-order network clustering framework is generally applicable to a wide range of network types, including directed, undirected, weighted, and signed networks.

REFERENCES AND NOTES

1. R. Milo *et al.*, *Science* **298**, 824–827 (2002).
2. S. Mangan, A. Zaslaver, U. Alon, *J. Mol. Biol.* **334**, 197–204 (2003).
3. J. Yang, J. Leskovec, *Proc. IEEE* **102**, 1892–1902 (2014).
4. P. W. Holland, S. Leinhardt, *Am. J. Sociol.* **76**, 492–513 (1970).
5. M. Rosvall, A. V. Esquivel, A. Lancichinetti, J. D. West, R. Lambiotte, *Nat. Commun.* **5**, 4630 (2014).
6. N. Pržulj, D. G. Corneil, I. Jurisica, *Bioinformatics* **20**, 3508–3515 (2004).
7. J. Leskovec, K. J. Lang, A. Dasgupta, M. W. Mahoney, *Internet Math.* **6**, 29–123 (2009).
8. Ö. N. Yaveroğlu *et al.*, *Sci. Rep.* **4**, 4547 (2014).
9. S. Mangan, U. Alon, *Proc. Natl. Acad. Sci. U.S.A.* **100**, 11980–11985 (2003).

10. C. J. Honey, R. Kötter, M. Breakspear, O. Sporns, *Proc. Natl. Acad. Sci. U.S.A.* **104**, 10240–10245 (2007).
11. S. E. Schaeffer, *Comput. Sci. Rev.* **1**, 27–64 (2007).
12. Minimizing $\phi_M(S)$ is nondeterministic polynomial-time hard (NP-hard), which follows from the NP-hardness of the traditional definition of conductance (28).
13. See the supplementary materials on Science Online.
14. Formally, when the motif has three nodes, the selected cluster S satisfies $\phi_M(S) \leq 4\sqrt{\phi_M^*} \leq 1$, where ϕ_M^* is the smallest motif conductance of any possible node set S . This inequality is proved in the supplementary materials.
15. The normalized motif Laplacian matrix is $L_M = D^{-1/2}(D - W_M)D^{-1/2}$, where D is a diagonal matrix with the row-sums of W_M on the diagonal [$D_{ii} = \sum_j (W_M)_{ij}$], and $D^{-1/2}$ is the same matrix with the inverse square roots on the diagonal [$D_{ii}^{-1/2} = 1/\sqrt{\sum_j (W_M)_{ij}}$]. The spectral ordering σ is the by-value ordering of $D^{-1/2}z$, where z is the eigenvector corresponding to the second smallest eigenvalue of L_M , i.e., σ_i is the index of $D^{-1/2}z$ with the i th smallest value.
16. C. Seshadhri, A. Pinar, T. G. Kolda, *Stat. Anal. Data Min.* **7**, 294–307 (2014).
17. R. Andersen, F. Chung, K. Lang, in *Proceedings of the 47th Annual IEEE Symposium on Foundations of Computer Science, FOCS'06*, Berkeley, California, 21 to 25 October 2006 (Institute of Electrical and Electronics Engineers, Piscataway, NJ, 2006), pp. 475–486.
18. J. J. Whang, I. S. Dhillon, D. F. Gleich, in *Proceedings of the 2015 SIAM International Conference on Data Mining*, Vancouver, British Columbia, Canada, 30 April to 2 May 2015, S. Venkatasubramanian, J. Ye, Eds. (Society for Industrial and Applied Mathematics, Philadelphia, PA, 2015), pp. 936–944.
19. A. Y. Ng, M. I. Jordan, Y. Weiss, *Adv. Neural Inf. Process. Syst.* **14**, 849–856 (2002).
20. D. Boley, *Data Min. Knowl. Discov.* **2**, 325–344 (1998).
21. D. L. Riddle et al., Eds., *C. elegans II* (Cold Spring Harbor Laboratory Press, Cold Spring Harbor, NY, ed. 2, 1997).
22. H. Lee et al., *Nat. Neurosci.* **15**, 107–112 (2011).
23. B. J. Frey, D. Dueck, *Science* **315**, 972–976 (2007).
24. B. Serrour, A. Arenas, S. Gómez, *Comput. Commun.* **34**, 629–634 (2011).
25. T. Michael, A. Joshi, B. Nachtergaele, Y. Van de Peer, *Mol. Biosyst.* **7**, 2769–2778 (2011).
26. A. R. Benson, D. F. Gleich, J. Leskovec, in *Proceedings of the 2015 SIAM International Conference on Data Mining*, Vancouver, British Columbia, Canada, 30 April to 2 May 2015, S. Venkatasubramanian, J. Ye, Eds. (SIAM, Philadelphia, 2015), pp. 118–126.
27. F. Krzakala et al., *Proc. Natl. Acad. Sci. U.S.A.* **110**, 20935–20940 (2013).
28. D. Wagner, F. Wagner, in *Mathematical Foundations of Computer Science 1993, Proceedings of the 18th International Symposium on Mathematical Foundations of Computer Science, MFCS'93*, Gdańsk, Poland, 30 August to 3 September 1993, A. M. Borzyszkowski, S. Sokolowski, Eds. (Lecture Notes in Computer Science, Springer, New York, 1993), pp. 744–750.
29. M. Kaiser, C. C. Hilgetag, *PLoS Comput. Biol.* **2**, e95 (2006).

ACKNOWLEDGMENTS

The authors thank R. Sosić for insightful comments. A.R.B. was supported by a Stanford Graduate Fellowship; D.F.G. was supported by NSF (CCF-1149756 and IIS-1422918), J.L. was supported by NSF (IIS-1149837 and CNS-1010921), trans-NIH initiative Big Data to Knowledge (BD2K), Defense Advanced Research Projects Agency [XDATA and Simplifying Complexity in Scientific Discovery (SIMPLEX)], Boeing, Lightspeed, and Volkswagen. Software implementations and the data sets used to obtain the results in this manuscript are available at <http://snap.stanford.edu/higher-order/>.

SUPPLEMENTARY MATERIALS

www.sciencemag.org/content/353/6295/163/suppl/DC1
Materials and Methods
Supplementary Text
Figs. S1 to S13
Tables S1 to S12
References (30–84)

18 November 2015; accepted 18 May 2016
10.1126/science.aad9029

PLANT SCIENCE

S-Acylation of the cellulose synthase complex is essential for its plasma membrane localization

Manoj Kumar,¹ Raymond Wightman,² Ivan Atanassov,^{1*} Anjali Gupta,¹ Charlotte H. Hurst,^{3,4} Piers A. Hemsley,^{3,4†} Simon Turner^{1†}

Plant cellulose microfibrils are synthesized by a process that propels the cellulose synthase complex (CSC) through the plane of the plasma membrane. How interactions between membranes and the CSC are regulated is currently unknown. Here, we demonstrate that all catalytic subunits of the CSC, known as cellulose synthase A (CESA) proteins, are S-acylated. Analysis of *Arabidopsis* CESA7 reveals four cysteines in variable region 2 (VR2) and two cysteines at the carboxy terminus (CT) as S-acylation sites. Mutating both the VR2 and CT cysteines permits CSC assembly and trafficking to the Golgi but prevents localization to the plasma membrane. Estimates suggest that a single CSC contains more than 100 S-acyl groups, which greatly increase the hydrophobic nature of the CSC and likely influence its immediate membrane environment.

Cellulose in plants is synthesized at the plasma membrane by the cellulose synthase complex (CSC), which contains at least 18 catalytic CESA protein subunits (1). The direction of CSC movement and the orientation of cellulose microfibril deposition are determined by cortical microtubules (2). Movement of the CSC through the plane of the plasma membrane is likely to cause severe disruption to the lipid bilayer (3), which suggests that membrane partitioning of this process may be important. Here, we describe the modifications of CESA proteins and demonstrate their importance to the functioning of the CSC.

S-Acylation involves reversible addition of an acyl group, often palmitate or stearate, to a cysteine residue, which can affect protein structure or localization (4). A recent study identified many S-acylated proteins in plants (5), including CESA1 and CESA3, which are essential for cellulose synthesis in the primary cell wall (6). We used acyl-resin-assisted capture (acyl-RAC) assays (7) to confirm that CESA1 is S-acylated (fig. S1) and showed that CESA6 is also S-acylated (Fig. 1A). Furthermore, all three CESAs required for cellulose synthesis in the secondary cell wall, CESA4, CESA7, and CESA8, are S-acylated (Fig. 1A), which demonstrates that S-acylation is a common feature of CESA proteins involved in cellulose synthesis in both primary and secondary cell walls.

CESA7 has 26 cysteines (fig. S2A). In order to identify S-acylated cysteines, we mutated indi-

vidual CESA7 cysteines to serines and tested their ability to complement the *cesa7^{trix3-1}* mutant. None of the eight cysteines in the zinc finger domain (ZR) showed any significant complementation (Fig. 2A and figs. S3 and S4). The structure of the RING-type zinc-finger domain from CESA7 [Protein Data Bank (PDB) ID: 1WEO] shows that all eight cysteines are involved in coordinating two zinc atoms, which makes them unlikely to be S-acylated. Consequently, we focused our subsequent analysis on other regions of CESA7. Two highly conserved cysteines in the short C terminus (table S1) are also essential for CESA protein function (Fig. 2A). None of the remaining 16 single cysteine mutants showed a substantial effect on cellulose content (Fig. 2A).

A cysteine-rich region lies within VR2 (8). The number of VR2 cysteines is conserved among orthologous CESAs from different species but varies between paralogous CESAs (table S1). There are four VR2 cysteines in CESA7 (fig. S2), and mutating them individually has no effect on cellulose biosynthesis (Fig. 2, A and C). We hypothesized that if VR2 is a site of CESA S-acylation, the remaining VR2 cysteines may support sufficient S-acylation for CESA7 function. Consequently, we mutated all four VR2 cysteines in CESA7 (VR2_{C/S}). The VR2_{C/S} mutant exhibited no complementation of *cesa7^{trix3-1}* (Fig. 2C). Thus, the cysteines in this region appear to be functionally redundant.

Having identified the VR2 and CT cysteines as potential S-acylation sites, we proceeded to determine if these sites were S-acylated. We generated a mutant in which both CT cysteines were mutated (CT_{C/S}). The CT_{C/S} mutant did not complement the *cesa7^{trix3-1}* mutant (Fig. 2B). Using Acyl-RAC assays we consistently found that S-acylation was dramatically reduced in the VR2_{C/S} mutant, although some signal remained. The CT_{C/S} mutants exhibited a smaller decrease in S-acylation (Fig. 1, B and C). We then constructed a mutant in which both the VR2 and CT cysteines were mutated

¹Faculty of Life Sciences, The University of Manchester, Michael Smith Building, Oxford Road, Manchester M13 9PT, UK.

²Microscopy Core Facility, Sainsbury Laboratory, University of Cambridge, Bateman Street, Cambridge CB2 1LR, UK.

³Division of Plant Sciences, School of Life Sciences, University of Dundee, Dow Street, Dundee, DD1 5EH, Scotland, UK. ⁴Cell and Molecular Sciences, The James Hutton Institute, Invergowrie, DD2 5DA, Scotland, UK.

*Present address: AgroBioInstitute, 8 Dragan Tzankov Boulevard, 1164 Sofia; Bulgaria. †Corresponding author. Email: simon.turner@manchester.ac.uk (S.T.); p.a.hemsley@dundee.ac.uk (P.A.H.)



Higher-order organization of complex networks

Austin R. Benson, David F. Gleich and Jure Leskovec (July 7, 2016)

Science **353** (6295), 163-166. [doi: 10.1126/science.aad9029]

Editor's Summary

Resolving a network of hubs

Graphs are a pervasive tool for modeling and analyzing network data throughout the sciences. Benson *et al.* developed an algorithmic framework for studying how complex networks are organized by higher-order connectivity patterns (see the Perspective by Pr ζ ulj and Malod-Dognin). Motifs in transportation networks reveal hubs and geographical elements not readily achievable by other methods. A motif previously suggested as important for neuronal networks is part of a "rich club" of subnetworks.

Science, this issue p. 163; see also p. 123

This copy is for your personal, non-commercial use only.

Article Tools Visit the online version of this article to access the personalization and article tools:
<http://science.sciencemag.org/content/353/6295/163>

Permissions Obtain information about reproducing this article:
<http://www.sciencemag.org/about/permissions.dtl>

Science (print ISSN 0036-8075; online ISSN 1095-9203) is published weekly, except the last week in December, by the American Association for the Advancement of Science, 1200 New York Avenue NW, Washington, DC 20005. Copyright 2016 by the American Association for the Advancement of Science; all rights reserved. The title *Science* is a registered trademark of AAAS.